Inorganic Coatings for Magnesium Alloys used in Orthopedic Implants

Eduardo Torres

eduardo.torres@tecnico.ulisboa.pt

Instituto Superior Técnico, Universidade de Lisboa, Portugal

January 2021

Abstract: Magnesium alloys, like AZ31, are nowadays investigated as potential materials for bioabsorbable implants, due to their mechanical properties that are closer to the ones of the human bones, and to the capacity of being corroded and absorbed inside the human body. The main issue related to these alloys is the high corrosion rate that will lead to the premature failure of the implant. Several studies have reported the possibility of reducing the corrosion rate by the application of bioabsorbable ceramic coatings. In this study this solution was explored by the application of the ceramic coatings using Plasma Electrolytic Oxidation (PEO) and Hydrothermal Treatment (HT). Other type of samples were coated with polycaprolactone (PCL) after the PEO treatment. All the samples were compared between each other and with the bare AZ31 alloy samples. Morphological and structural analysis were performed by Scanning Electron Microscopy (SEM) and X-Ray Diffraction (XRD) techniques. The corrosion behavior of the samples was tested with Electrochemical Impedance Spectroscopy (EIS) in SBF solution, with the best results corresponding to the PEO+PCL association, followed by the PEO+HT. The biological survival rate of fibroblasts when in contact with the samples was evaluated by fluorescence, indicating that the coating with best performance is the PEO+HT. Thus, the PEO coating followed by hydrothermal treatment has proven to be the best candidate for applications where a controlled degradation of bioabsorbable implants is envisaged.

Keywords: AZ31; Hydroxyapatite; Orthopedic Implants; Plasma Electrolytic Oxidation (PEO); Hydrothermal Treatment; Dip-Coating; Polycaprolactone (PCL); Electrochemical Oxidation Spectroscopy (EIS)

1. Introduction

The materials used nowadays for the production of implants are biocompatible, meaning that their presence inside the body causes no adverse reaction on the organism but also doesn't offer any benefit, beside of the healing of the fractures and support functions. The materials more commonly used (cobalt, titanium and its alloys and stainless steel) have mechanical properties that are highly distinct from the ones of the human bone, especially density and Young's modulus, leading to potential problems like the stress shielding, that can compromise the bone structure. Moreover, they also require a second surgery for the removal of the implant. **[1, 2]**

With the use of magnesium alloys we assist to a change of paradigm since magnesium and some of its alloys are bioabsorbable. Even more important, the mechanical properties of these alloys are closer to the ones of the human bones. The corrosion products of the implants can be excreted or absorbed by the human organism (highlight for the Mg^{2+} and Ca^{2+} that are locally consumed for the bone healing process). Although the high corrosion rate of these alloys is the main obstacle to their use, since it is mandatory to ensure that the implant can perform its role during the period necessary for the bone healing process (12-18 weeks), and also that the quantity of the products released during the degradation is non-toxic for the human body. **[3, 4]**

One possible solution to this problem is the application of a ceramic, non-toxic, coating on top of the bare alloy in order to delay its corrosion rate. The hydroxyapatite coating, produced through PEO and Hydrothermal Treatment, was reported for several scientists as a coating that allows to protect the substrate from the corrosive environment, being at the same time biocompatible and porous. The porosity is useful to promote the cellular adhesion and can be tailored by controlling the processing parameters. The chemical composition of these coatings includes some elements like Mg and Ca that are useful to the bone regeneration process.

The evaluation of the corrosion resistance of these materials is of highly importance and should be deeply studied in mediums that simulate the body fluids, like the SBF (Simulated Body Fluid). Also, osseointegration and biocompatibility should be deeply studied *in vitro* in order to identify the cellular behaviour in the presence of the implant materials and corrosion products. **[5]**

2. Experimental Procedure

2.1 Sample Preparation

From a 25 mm diameter AZ31 rod (from Goodfellow), 40 disks of 6 mm thickness were cut using the Electrical Discharge Machining technique to avoid the exposure to high temperatures and the development of stresses on the samples. To establish the electric connection, the back of each sample was polished with a P1200 SiC paper, rinsed with Millipore® water and ethanol, and dried with an air blower. Then, a copper wire was glued on that surface with SPI® silver paint. The samples were then inlayed in Epofix epoxy resin from Struers®. After drying, a hole was drilled on the side of the samples to easier the fixing for the next steps. The samples were numbered and polished with P320, P600, P1200 and P2400 SiC papers, rinsed with Millipore® water and ethanol, and dried with an air blower.

Among the samples submitted to PEO treatment, 12 were afterward submitted to Hydrothermal Treatment and 10 were coated with PCL by Dip-Coating. Some bare AZ31 samples were also kept to be characterised or used as control.

2.2 Plasma Electrolytic Oxidation (PEO)

An Agilent® 6813B AC source was used. The cell was composed by a 1L glass beaker and a 316 stainless-steel tubular coil through which circulated oil at 10±0.5°C, powered by a Julabo® refrigerator. The following parameters were used: duty cycle of 20%, V_{rms}=160V, V_{DC}=80V, frequency=100Hz, I_{limit}=0.6A, I_{peak}=26A, agitation of 350 rpm, and a total process time of 600s. The 600mL solution used had the composition mentioned in the table 1.

Table 1: Solution used for PEO treatment

Reagents	Concentration (g/L)
Na_3PO_4	20.0
$Ca(OH)_2$	2.0

After the treatment the samples were rinsed with Millipore® water, ethanol and dried with an air blower. The thickness of the coating was measured with an Elcometer® thickness gauge.

2.3 Hydrothermal Treatment

A double wall glass cell was used together with a Julabo® Heating Immersion Circulator. The temperature was set to 90±0.5°C, the treatment last for 4 hours and the solution described in table 2, tuned to a pH=8.5, was used.

Table 2: Solution used for Hydrothermal Treatment

Reagents	Concentration (g/L)
KH_2PO_4	13.609
EDTA(Ca)	37.628

The samples were rinsed in water and ethanol, dried with an air blower and the thickness of the coating was measured with the Elcometer® thickness gauge.

2.4 Dip-Coating

The solution described in table 3 was prepared in a 50mL glass beaker.

Table 3: Solution used for Dip-Coating treatment

Reagents	Concentration (g/L)
Polycaprolactone (PCL)	26.56
Chloroform	(solvent)

The two components were mixed for 2 hours with a magnetic stirrer. The samples were dipped using a Bungard RDC 15 dip coater with the treated face perpendicular to the solution, remained dipped for 60 seconds and were removed from the solution at a velocity of 1,4 mm/s. The samples were kept in ambient conditions for 24 hours and then stored in a desiccator.

2.5 Morphological and Structural Analysis

2.5.1 Metallographic analysis

The bare AZ31 sample was polished to P4000 SiC paper, followed by 3 μm diamond suspension in appropriate cloth and OPS under running distilled water, for 2 minutes. The samples were rinsed with water and soap, ethanol and dried with an air blower. The samples were etched with a Picral solution: 10mL of acetic acid (99%), 4.2g of picric acid, 10mL of distilled water and 70 mL of ethanol (75%), for 6 seconds. The etching was stopped in running water. The samples were then rinsed with Millipore® water and ethanol and dried with an air blower. The metallographic analysis was performed on a Leica® DM 2700M optical microscope. The mean grain area and diameter were measured with the *software* ImageJ.

2.5.2 X-Ray Diffraction

The analysis was performed on a X-Ray Philips® PW diffractometer with CuK_α radiation tube, with a wavelength of 1.542Å, potential difference of 40kV, current 30mA, an increment of 0.05^0, with a measure at every 0.5s. The data were analysed

with the Match! Software (version 3.11.0.180) and the Crystallography Open Database (COD). The PCL peaks used for comparison are the ones presented by Rezaei and Mohammadi **[6]**.

2.5.3 Scanning Electron Microscopy

One sample of each type (PEO; PEO+Hydrothermal; PEO+PCL) was analysed both on top and on the cross section on the Hitachi® S2400 Scanning electronic microscope equipped with an EDS Bruker® light elements detector. The samples were coated with a thin conductive layer of Au-Pd.

2.6 Cellular Assays

Fibroblasts ATCC L-929 were grown on a cell culture medium "Dulbecco's Modified Eagle Medium" (DMEM) supplemented with 10% of bovine fetal serum (FBS) and penicillin/streptomycin 100U/mL, at 37^{0}C in humidified atmosphere with 5% CO_2. When the growth presented 80% of confluence, the medium was removed and the flask was washed with a 0.25% trypsin solution, followed by a 10 minutes incubation with more trypsin solution at 37^{0}C for the cells to loosen from the flask walls. The actuation of trypsin was verified on the inverted optic microscope. Was added DMEM medium to inhibit the trypsin effect, by the FBS action. The medium with the cells was pipetted to a tube, was homogenized by smooth pipetting, the aggregates were broken, the cells were counted on a "Neubaeur" chamber and the concentration was tuned to 50× $\mathbf{10^5}$ cells/mL. One millilitre of cellular suspension was pipetted to the top of the samples previously rinsed with ethanol and placed on 6 well-plates, 1 well was used as control. After 2 hours more 3 mL were added on each well, leaving the samples submerged. The samples were introduced on the stove at 37ºC, with humidified atmosphere and 5% CO_2. After 24 hours the medium with no signs of infection was removed and substituted by 4mL DMEM medium with 10% (v/v) of PrestoBlue®, the samples were placed on the stove at 37ºC, with humidified atmosphere and 5% CO_2. Three and half hours later a 100 microliter sample was collected from each well and placed on a 96 well plate. The fluorescence was measured, by comparison with a blank sample, on a FilterMax® F5 Multi-Mode Microplate Reader, for excitation at 535 nm and emission at 625 nm. The statistical analysis of the cell viability was done by the analysis of the means and standard deviations for each type of sample. The analysis of variance was performed by the "One Way Analysis Of Variance" (ANOVA) method, was used α=0.05 and $p>0.05$ as statistically significant. The post-hoc analysis was performed by the Tukey's method.

2.7 Electrochemical Impedance Spectroscopy

The corrosion behaviour of the samples was assessed by a Gamry® 600+ potentiostat and the Gamry® Framework software. A three electrode cell was used, with the sample being the working electrode, a saturated calomel electrode as reference and a platinum coil as counter electrode. The solution used to simulate the body fluids was the SBF (Simulated Body Fluid), present on table 4. Potential perturbations with an amplitude of 10mV rms, frequency range from 50 kHz to 10 mHz, with 7.13 points per decade, were used. The impedance measurements were performed at 5 moments after the immersion of the sample in the SBF solution: 1, 24, 48, 72 and 168 hours. The cell was maintained inside a Memmert HPP 260 climate chamber (that also worked as Faraday cage) at a constant temperature of 37ºC during the whole process. At the end of immersion, the samples were rinsed with Millipore® water and ethanol, dried with an air blower and were stored in a desiccator.

Table 4: Concentrations of the SBF solution

Reagents	Concentration (g/L)
NaCl	7.996
$NaHCO_3$	0.350
KCl	0.224
$K_2HPO_4 \cdot 3H_2O$	0.228
$MgCl_2 \cdot 6H_2O$	0.305
HCl (1M)	40mL
$CaCl_2$	0.278
Na_2SO_4	0.071
$(CH_2OH)_3CNH_2$	6.057

3. Results and Discussion

3.1 Metallographic Analysis

The optical microscopy analysis is presented in figure 1. The microstructure is constituted by only one phase, the Mg-α solid solution.

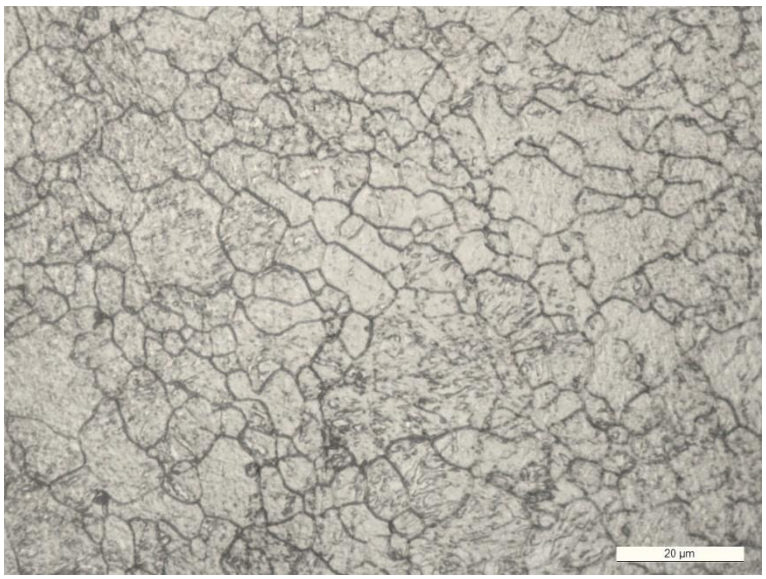

Figure 1: Optic microscopy image of the AZ31 alloy

The mean grain area measured with the ImageJ *software* was: 35.78 μm^2, with a standard deviation of 37.54 μm^2. With the value of the area the grain mean diameter was obtained: 6.75 µm, which is equivalent to a 12 ASTM grain size.

3.2 Thickness of the coatings

The measurements made with the Elcometer® thickness gauge resulted on a PEO average thickness of 66.2 µm, and the measurements after Hydrothermal Treatment resulted on a total coating thickness of 69.0 µm. Thus, the hydrothermal treatment results in a thickness increase of 2.8 µm in comparison with the PEO coating. The measurements show a reduced standard deviation, which was attributed to a homogeneous thickness of the coating.

3.3 X-Ray Diffraction (XRD)

The analysis of figure 2 allows to identify the compounds present in each sample. The pattern for the bare AZ31 revealed the presence of Mg-α phase, being coherent with the metallographic analysis. Magnesium oxide (MgO) and magnesium hydroxide ($Mg(OH)_2$) were also identified, the lower intensity of these peaks being related with the thin oxide layer formed. The pattern for the PEO treated sample revealed magnesium (Mg), magnesium oxide (MgO), magnesium hydroxide ($Mg(OH)_2$) and magnesium phosphate ($Mg_3(PO_4)_2$) peaks, this latter compound being due to the incorporation of PO_4^{3-} ions from the electrolyte.

The XRD pattern of the PEO+Hydrothermal treated sample allowed to identify Mg, MgO, $Mg(OH)_2$, $Mg_3(PO_4)_2$ (less quantity than for the PEO sample), together with hydroxyapatite peaks. The presence of this compound is explained by the modification of the coating in contact with the Hydrothermal Treatment electrolyte, with the calcium being the main element to get incorporated on the ceramic coating with this treatment. The PEO+PCL coating revealed the peaks identified for the PEO sample, plus some slight change in the intensity of the peaks at 15.7º; 21.5º; 23.8º, that is not noticeable just by the general analysis of the figure, and that is characteristic of the PCL compound (semi crystalline polymer). **[6]** These peaks are masked by the Mg_3PO_4 ones, since they are coincident, and the lower intensity was attributed to the lower quantity of PCL that was deposited on the samples (monolayer of lower thickness).

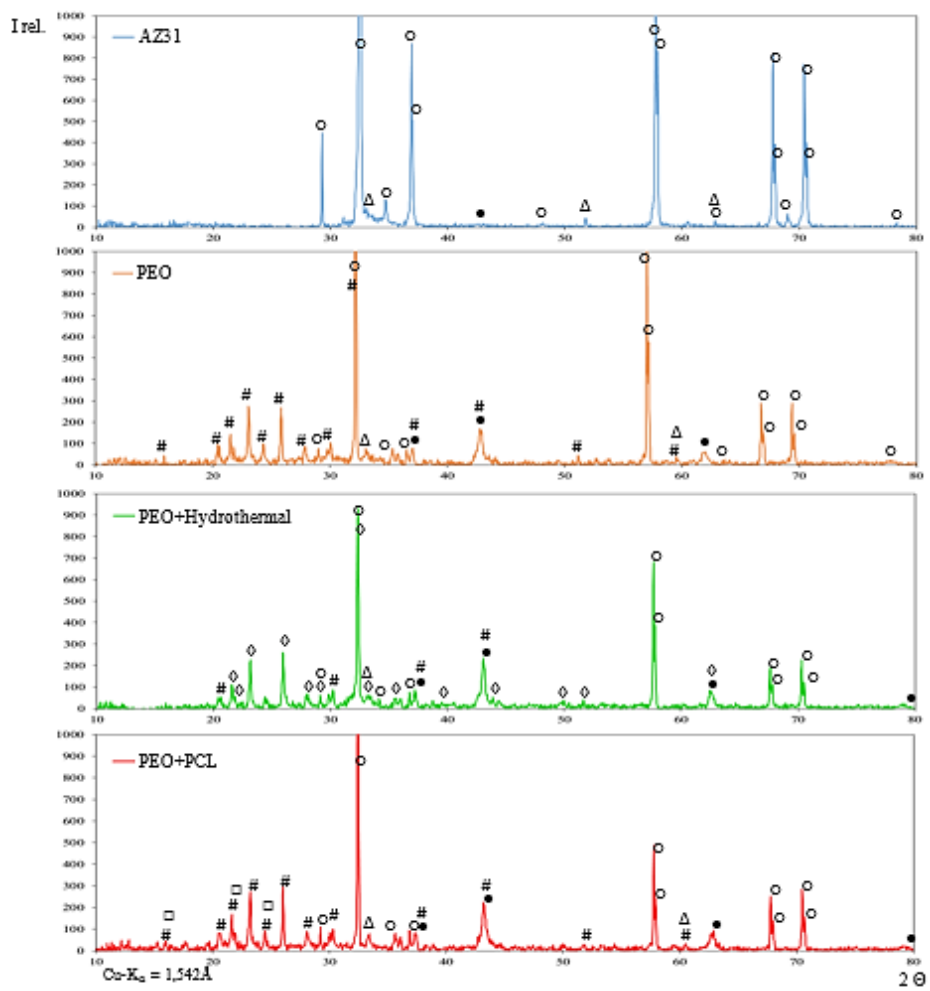

Figure 2: XRD patterns for the 4 types of samples used: AZ31; PEO; PEO+Hydrothermal; PEO+PCL. The symbols used to identify the peaks correspond to: ○ – Mg; ● – MgO; Δ – $Mg(OH)_2$ # – Magnesium Phosphate; ◊ - Hydroxyapatite; □ - PCL

3.4 Scanning Electron Microscope

The SEM analysis allowed to identify that the surface pores of the PEO samples (with a distribution of diameters with mean value of 25 μm) have a larger diameter than those of the PEO+Hydrothermal samples (mean value of 22 μm), showing that the hydrothermal treatment results in a reduction of the pores diameter, perhaps even sealing completely the smaller pores. Furthermore, the PEO sample show higher range of pore sizes. The PEO+PCL sample have polymeric fibres (PCL) dispersed all along the surface. These fibres were assumed to be PCL fibres that were not completely homogenized during the dip-coating solution preparation. This could be solved by the increase of the agitation time or by the application of ultrasonic stirring. Cracks were identified in all the samples, which can be formed during the PEO treatment due to the temperature difference between the plasma discharge and the electrolyte temperature, or due to the vacuum that is necessary for the SEM analysis.

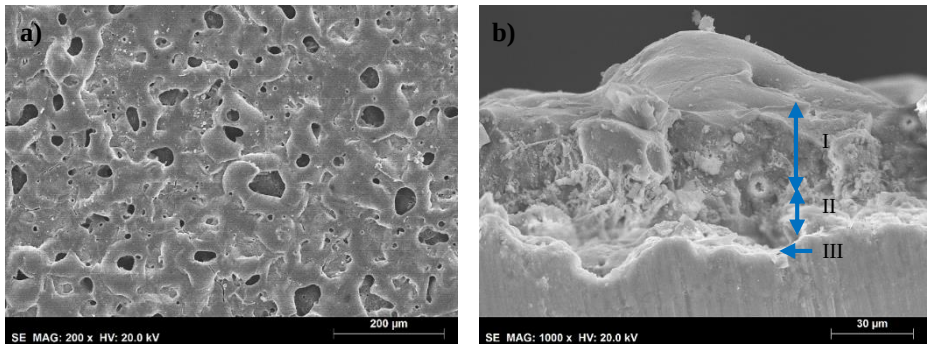

Figure 3: PEO sample. a) Surface; b) Cross section. I- Top layer; II- Middle layer; III- Bottom layer

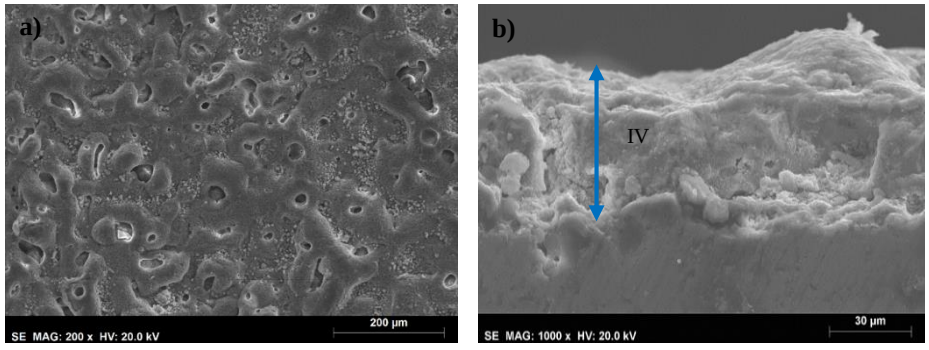

Figure 4: PEO+Hydrothermal sample. a) Surface; b) Cross section. IV- Coating

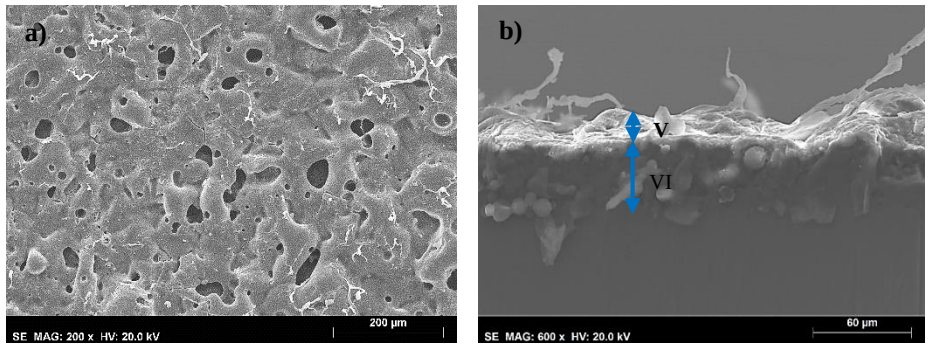

Figure 5: PEO+PCL sample. a) Surface; b) Cross section. V- PCL coating; VI-PEO coating

Smaller pores inside the superficial ones were identified in all the coated samples, showing that interconnectivity of the pores may exist. The EDS analysis (table 5) of the AZ31 sample revealed low amount of oxygen, which can be interpreted as a thin layer of MgO and $Mg(OH)_2$ formed on the surface, agreeing with the XRD results. The EDS of the PEO sample revealed the presence of the elements: Mg, O and P, so, the surface should be constituted mainly by: MgO and magnesium phosphates. The ratio Ca/P (0.035) allowed to notice that no hydroxyapatite was formed in this treatment, agreeing once again with the XRD results. In fact, the incorporation of Ca^{2+} in the coating is not expected, due to the net positive charge of the electrode during PEO.

The EDS of the PEO+Hydrothermal sample surface allowed to identify the elements: O, Ca and P, indicating the formation of calcium phosphates, of which hydroxyapatite is an example. Although, the Ca/P ratio had a value of 1.354 that is not yet the characteristic value of the crystallographic hydroxyapatite (Ca/P=1.67). The pre-existence of phosphorous in the PEO coating can mask the presence of hydroxyapatite by changing the ratio between calcium and phosphorous.

The EDS of the PEO+PCL sample revealed higher amounts of C when compared with the PEO sample, which is explained by the PCL ($[C_6H_{10}O_2]_n$) layer. The analysis made on the brighter regions revealed higher concentrations of C and lower concentrations of O, when compared with the darker regions of the surface. Anyway, in all the surface the amount of C was higher than on the PEO sample surface, demonstrating that the PCL covers all the surface.

Table 5: Atomic % of the elements identified on the SEM-EDS for each sample

Samples	Elements (% At)							
	Mg	Al	Zn	O	C	P	Na	Ca
AZ31	95.5	1.19	1.93	1.39	-	-	-	-
PEO (39)	19.39	-	1.6	43.18	20.83	10.12	4.51	0.36
PEO+Hydrot. (6)	3.32	0.18	-	43.83	16.62	14.62	1.62	19.8
PEO+PCL (12)	11.36	0.2	-	31.7	47.7	6.41	2.62	-

The cross section of the PEO sample allowed to distinguish 3 different layers: a bottom dense and thin layer, a middle layer with some porosity, and a top layer that is thicker and more porous, with the pores having a larger diameter than the ones present on the middle layer (figure 3b)). The linear EDS analysis revealed an abrupt decrease of Mg concentration in the interface between the substrate and the bottom layer. Associated to this decrease, an increase in oxygen and phosphorous was detected. Phosphorous concentration remains constant while oxygen decreased along the coating thickness. The decrease of magnesium and oxygen along the thickness of the coating suggests higher concentration of magnesium oxides in the bottom and middle layers than in the top one. At the same time, the phosphate concentration seems to remain constant. The total thickness of the coating is lower

than the thickness measured with the Elcometer® thickness gauge. The results presented on the table 6 demonstrate that the bottom layer is the thinner, the intermediate layer is the middle one also in thickness, and the top layer is the thicker.

Table 6: Thickness of the 3 layers identified for the coating of the PEO sample, and total thickness value. Each value result from an average of 20 measurements

PEO Sample		
	Average (µm)	**Standard Deviation (µm)**
Bottom Layer Thickness	2.40	1.10
Middle Layer Thickness	16.83	6.79
Top Layer Thickness	33.96	4.96
Total Thickness	**53.19**	**7,19**
Elcometer thickness	67.3	4.8

The cross section of the PEO+Hydrothermal sample allowed to measure the total thickness of the coating (table 7), that revealed to be lower than the one measured on the Elcometer. The value of the standard deviation reflects a non-uniformity of the thickness, as can be seen on figure 4b). The EDS analysis was identical to the one made to the PEO sample, with the difference of the lower concentrations of magnesium registered along all the thickness of the coating. Ca and P were also detected, indicating the formation of calcium phosphates. The point analysis revealed a ratio Ca/P=1.57 that is characteristic of calcium-deficient hydroxyapatite **[7]**. Once again, is important to refer that the pre-existence of P in the PEO coating, in the form of magnesium phosphates, can affect the detection of the correct Ca/P ratio. The result of the presence of hydroxyapatite is coherent with the XRD for this sample.

Table 7: Hydrothermal Treatment coating thickness. The values result from an average of 20 measurements

PEO+Hydrothermal Sample		
	Average (µm)	**Standard Deviation (µm)**
Total Thickness	54.40	7.64
Elcometer Thickness	71.2	6.3

The cross section of the PEO+PCL samples allowed to distinguish between the PEO and the PCL coatings. The spherical particles distinguishable on the figure 5 b) were identified as SiC particles from the sandpapers used in the preparation of the samples. The EDS has shown the same elements behaviour as in the PEO coating. In the brighter zone the concentrations of O and C increased, being that coherent with the presence of PCL.

3.5 Cellular Assays

The cellular assays revealed that the survival rate of the fibroblast cells after 24 hours in contact with the samples (figure 6) follows the order: AZ31 > PEO+Hydrothermic > PEO+PCL > PEO. In spite of AZ31 showing the better result for this test, the corrosion behavior of the samples prevents its use without any surface treatment as orthopedic implant.

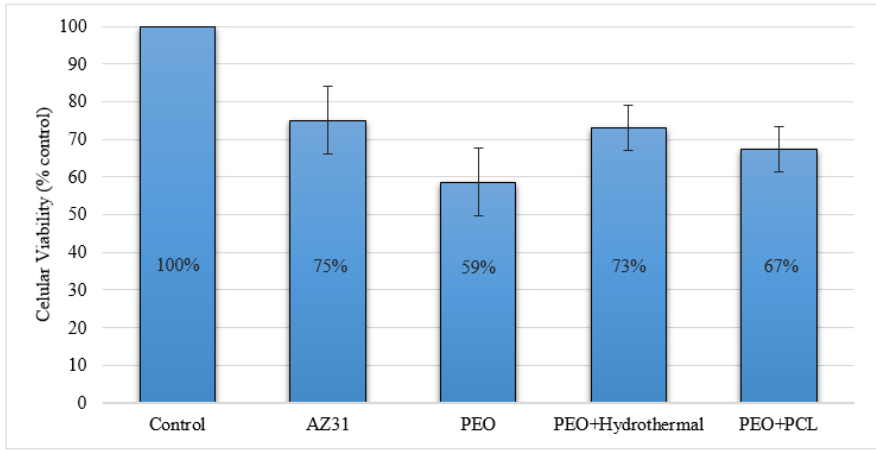

Figure 6: Cells survival rate in each type of sample. The values for each type of sample result from an average of 3 values

According with the same data, PEO+Hydrothermal samples show a result that is almost as good as for the AZ31 samples, so the PEO+Hydrothermal process seems to be the best solution for the biomedical implants.

The analysis of variance (ANOVA) revealed that the "p-value" is lower than α=0.05 and so, the null hypothesis was rejected (the mean values for each type of samples are all equal). For the same analysis the "F-Value" was higher than "F-crit", and so, the "F-value" is inside of the rejection region, and once again, the null hypothesis can be rejected, for α=0.05. This information indicates that a statistical difference between the types of samples exists. **[8]**

The post-hoc Tuker method revealed the existence of a significant statistical difference between the control and each type of samples (AZ31, PEO; PEO+Hydrothermal; PEO+PCL), and that no significant statistical difference existed between the types of samples (AZ31, PEO; PEO+Hydrothermal; PEO+PCL), for α=0.05.

3.6 Electrochemical Impedance Spectroscopy

The impedance for the AZ31 sample was measured for 24, 48 and 168 hours, being represented on the figure 7.

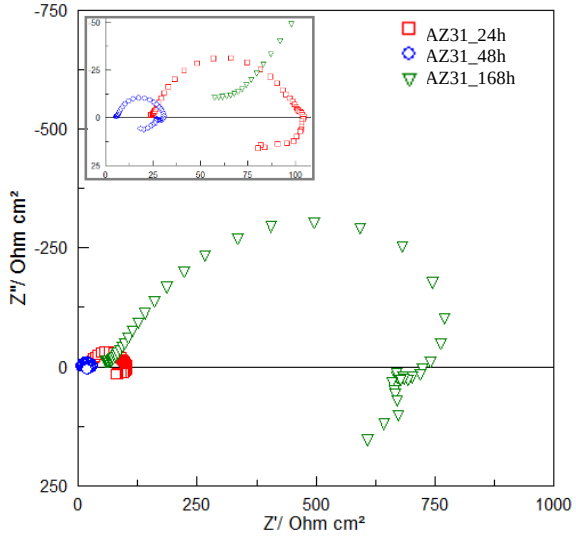

Figure 7: Nyquist diagram for the impedance of the AZ31 sample

Figure 7 denotes an evolution of the impedance to higher values with time. The shape of the three curves is identical and is constituted by three loops: one capacitive loop almost imperceptible, at higher frequencies, usually associated with the presence of an oxide film or corrosion products, a capacitive loop for medium frequencies, associated with the charge transfer during the corrosion process, and an inductive loop for lower frequencies, that is frequently used to describe the corrosion kinetics of magnesium and its alloys. One equivalent circuit that can describe the AZ31 behavior was proposed by Bland *et al* **[9]** and is constituted by a resistance (R_0) that represents the solution resistance, two ladder RC circuits (R1/C1 and R2/C2) and, in parallel, an association of a resistance (R3) and an inductor (L1). The corrosion products film is represented by the capacity of the film (C1) and by the additional solution resistance inside the pores (R1). The active area of the material, where corrosion takes place, is located at the bottom of the pores and is represented by the charge transfer resistance (R2) and the double layer capacitance (C2). Finally, the inductive response is represented by the R3 and L1 elements. The equivalent circuit used to fit the results of the AZ31 samples was modified from the circuit proposed by Bland *et al* **[9]**, with the elements C1 and C2 being replaced by constant phase elements (CPE) in order to take into account the deviations from the ideal behavior. The circuit is represented on figure 8 and allowed to obtain an excellent fitting to the results, with χ^2 equal or lower than 10^{-3}. The polarization resistance for the AZ31 sample is also represented on the figure 8.

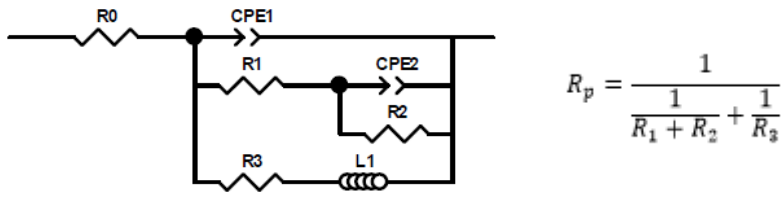

Figure 8: Equivalent circuit for the AZ31 sample and respective R_p formula

Impedance spectra for the PEO samples were measured for 1, 24, 48, 72 and 168 hours, being represented on figure 9.

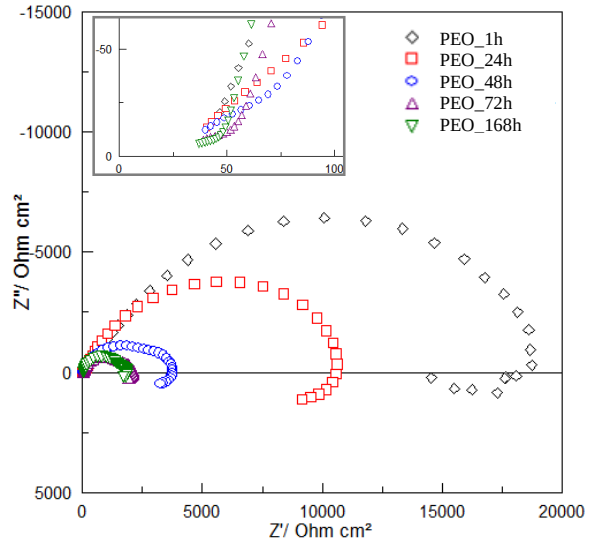

Figure 9: Nyquist diagrams for the impedance of the PEO sample

The Nyquist diagrams of the PEO samples show that the impedance values decrease with immersion time on the SBF solution. The shape of the diagrams remains identical with the time, being characterized by four loops: three capacitive loops for high and medium and medium-low frequencies, and one inductive loop for lower frequencies. The equivalent circuit used (figure 10) is identical to the one used for the AZ31 samples, but one more ladder RC circuit was added after R2. In this equivalent circuit, adapted from other equivalent circuit proposed by Bland *et al* **[9]**, the PEO coating is represented by R1 and CPE1 that stand for the additional solution resistance inside the pores of the coating and the capacitance of the coating, respectively. The ladder R2/CPE2 and R3/CPE3, and the serial R4-L1 constitute the equivalent circuit used for the AZ31 sample that was previously explained. The equivalent circuit presented on figure 10 allowed to obtain an excellent fitting of the experimental results, which was confirmed by the χ^2 values. The polarization resistance for the PEO sample is also represented on the figure 10.

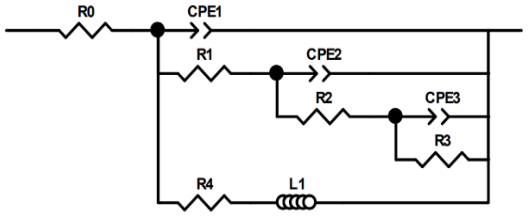

$$R_p = \frac{1}{\frac{1}{R_1 + R_2 + R_3} + \frac{1}{R_4}}$$

Figure 10: Equivalent circuit for the PEO and PEO+Hydrothermal samples, and respective R_p formula

The impedance for the PEO+Hydrothermal samples was measured for 24, 48, 72 and 168 hours, being represented on the figure 11. For these samples the impedance values also decrease with the time as for the PEO samples.

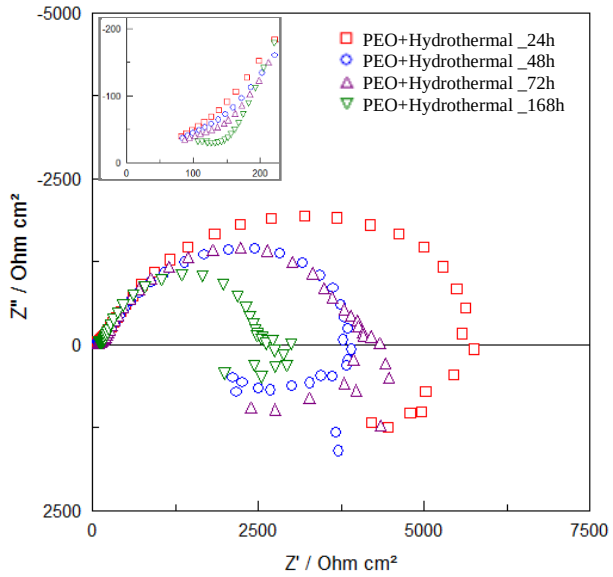

Figure 11: Nyquist diagram for the PEO+Hydrothermal sample

The Nyquist diagrams for the PEO+Hydrothermal samples are identical in shape, with the 48 and 72 hours curves being overlapped. The behavior of the PEO+Hydrothermal samples is identical to that registered for the PEO samples and consequently, the equivalent circuit and polarization resistance used for the PEO samples were used also for the PEO+Hydrothermal samples (figure 10). Once again the fitting obtained to the experimental results was excellent.

The impedance for the PEO+PCL samples was measured for 1, 24, 48, 72 and 168 hours, being represented on the figure 12. For this samples the impedance values also decrease with time, as for the PEO and PEO+Hydrothermal samples.

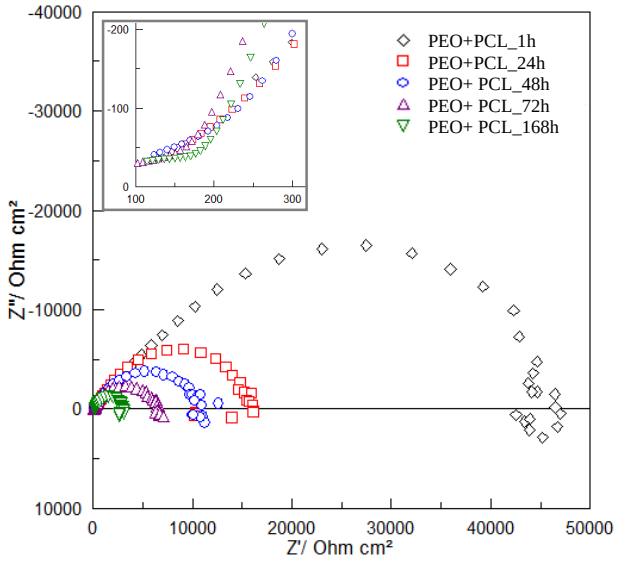

Figure 12: Nyquist diagram for the PEO+PCL sample

The shape of the Nyquist diagrams was identical for all spectra, being constituted by four loops: three capacitive loops for the higher, medium and medium-low frequencies, and an inductive loop for the lower frequencies. The behavior of the PEO+PCL samples was distinct from the one of the PEO samples and for that reason a new equivalent circuit was considered (figure 13). The equivalent circuit can be decomposed in two parts: R1/CPE1, that represent the PCL layer (R1 is the solution resistance inside the pores of the PCL coating and CPE1 the capacitance of the coating), and the circuit that describes the corrosion behavior of the AZ31 sample (figure 8). The two parts of the equivalent circuit are in ladder configuration. The polarization resistance for the PEO+PCL sample is represented on the figure 13.

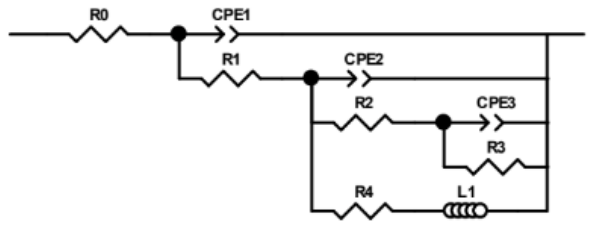

$$R_p = R_1 + \frac{1}{\frac{1}{R_2 + R_3} + \frac{1}{R_4}}$$

Figure 13: Equivalent circuit for the PEO+PCL samples, and respective R_p formula

When the SBF solution penetrates the pores of the PCL coating, it attacks the PEO coating that is underneath, increasing the size of the pores and infiltrating to the substrate, which will be corroded. The results obtained with the fitting of this circuit to the experimental results were excellent.

A summary of the electrochemical impedance spectroscopy results through the average values of the polarization resistance obtained for each type of samples is presented in table 8.

Table 8: Variation of the mean Rp value with time for all the samples

Samples	Time				
	1h	24h	48h	72h	168h
R_p (Simples) (Ω cm^2)	—	5.15E+1	1.10E+2	—	5.90E+2
R_p (PEO) (Ω cm^2)	1.95E+4	8.75E+3	3.10E+3	1.80E+3	1.50E+3
R_p (PEO+Hydrot.) (Ω cm^2)	—	6.20E+3	4.25E+3	3.05E+3	1.75E+3
R_p (PEO+PCL) (Ω cm^2)	4.65E+4	2.45E+4	9.65E+3	4.70E+3	2.50E+3

The analysis of table 8 allows to conclude that any of the produced coatings increases the polarization resistance of the AZ31 sample, indicating that all the coatings confer protection to the substrate. Overall, the PEO treatment increases significantly the corrosion resistance of the AZ31. When compared with the PEO+Hydrothermal sample, a higher polarization resistance for the first immersion moments is obtained for the PEO samples, although for 48 hours the R_p value is already lower than the one for PEO+Hydrothermal samples. This behavior can be explained by the hydration of the oxides: the PEO samples were immersed in the SBF solution in the state they obtained after the PEO treatment, with the oxide being only slightly hydrated, whereas the hydrothermal treatment of the PEO+Hydrothermal samples promoted the hydration of the oxide, and so, when the PEO+Hydrothermal samples were immersed in the SBF solution, the were already hydrated. For this reason, it is expected that the variation of R_p for the PEO+Hydrothermal samples is less significant than for the PEO samples. However, for longer periods the protection of the PEO+Hydrothermal is more effective than the one of the PEO treatment.

The analysis of the same table also allows to conclude that the PEO+PCL sample presents the higher values of all the coatings for all the immersion times in the SBF solution. This way, the PEO+PCL coating is the one that confers the highest corrosion protection, in spite of its biodegrability. The data of table 8 were represented graphically in figure 14. Only immersion times equal or higher than 24h were considered.

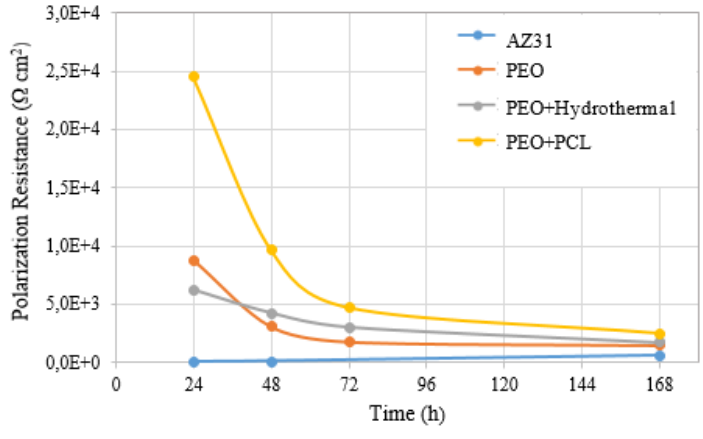

Figure 14: Variation of the mean Rp value with time for all the samples

Figure 14 allows to notice the decrease of the polarization resistance with the time for the PEO, PEO+Hydrothermal and PEO+PCL samples and the opposite behavior for the AZ31 samples. It is also notorious the inversion of positions of the PEO+Hydrothermal and the PEO samples, somewhere between the 24 and the 48 hours, showing an improved behavior of the PEO+Hydrothermal process. Finally, is evident that the PEO+PCL samples have the higher values for the polarization resistance along all the considered period of immersion in the SBF.

4. Conclusions

The demand for bioabsorbable materials imposes the need for studying new alloys and coatings to guarantee that the implant materials comply with the mechanical requirements when needed and are gradually absorbed by the human body. The corrosion rate of these materials presents the biggest challenge. Controlling the corrosion rate will allow to reduce the inflammation and rejection, at the same time ensuring that the release of ions takes place within its concentration limit in the human body. In this work three coatings (PEO; PEO+HT; PEO+PCL) were tested in order to increase the corrosion resistance. This study included the metallographic characterization of the alloy, the structural and morphological characterization of the produced coatings, as well as the study of the corrosion resistance through electrochemical impedance spectroscopy and the cellular viability of the coatings.

The results obtained are summarized below:

• The metallographic analysis of the AZ31 alloy revealed the presence of only one phase (Mg-α) and a medium grain diameter of 6.75 μm which corresponds to an ASTM 12 grain size.

• The X ray diffraction confirmed the results of the metallographic analysis for the AZ31 sample, and revealed also the presence of MgO and $Mg(OH)_2$. Magnesium phosphate ($Mg_3(PO_4)_2$) was identified in all the coatings, this compound being

produced during the PEO treatment. The presence of hydroxyapatite was identified on the PEO+Hydrothermal sample and for the PEO+PCL sample the presence of polycaprolactone (PCL) could be detected.

• The thickness measurements performed with the Elcometer® revealed an increase of the total thickness of the coating with the hydrothermal treatment, after the PEO treatment.

• The SEM analysis revealed perfectly coated surfaces, with a uniform and porous coating. In this analysis it was possible to measure the pore size and conclude that the hydrothermal treatment resulted in a decrease of the pores average diameter. Interconnectivity of the pores was identified in all coatings. The PEO+Hydrothermal samples revealed the presence of small spherical structures on the surface and the compositional analysis (EDS) of the coating revealed a Ca/P ratio that is characteristic of hydroxyapatite.

• The cellular viability assays revealed that the cells survival rate was higher for the AZ31 samples, although the corrosion problems of this alloy make unfeasible its without any coating. From the coatings studied, the PEO+Hydrothermal let to the best results, with a survival rate that is just 2 percent lower than the one of the AZ31 samples.

• Electrochemical impedance spectroscopy revealed that the PEO+PCL coating is the one that presents the best results for all the immersion times (until 168h). Nevertheless, for 168 hours the polarization resistance of the three coatings was of the same order of magnitude, with the PEO+Hydrothermal coating being the second best.

• The presence of hydroxyapatite, the decrease of the porosity and the highest cellular viability, associated with the second best corrosion resistance, determine that the PEO+Hydrothermal coating is the one that presents the best overall performance. Even though, the behaviour of the PCL coating should not be disregarded and this polymer should be considered to be used on top of PEO+Hydrothermal treatment if a higher corrosion resistance of the coating is needed.

This work demonstrated that it is possible to obtain a uniform coating that improves the corrosion resistance of the AZ31 alloy, without the cellular viability being practically compromised. Further studies should be performed, starting with the PEO+Hydrothermal system, to evaluate the mechanical behaviour and allow complementary evaluations of the biological behaviour of this coating, in order to ascertain the possibility of applying it on the bioabsorbable implants of the future.

5. References

[1] M. Kiselevsky, N.Yu.Anisimova, B. Polotsky, N.S.Martynenko, E.A.Lukyanova, S. Sitdikova, S. Dobatkin and Y. Estrin, "Biodegradable Magnesium Alloys as Promising Materials for Medical Applications (Review)," *Sovremennye Tehnologii v Medicine,* vol. 11 Nº3, 2019.

[2] F. P. S. d. Albuquerque, "Magnesium AZ31 alloy coating for bone implant applications," Dissertação de Mestrado em Engenharia de Materiais. Instituto Superior Técnico, Lisboa, 2018.

[3] S. Chatterjee, M. Saxena, D. Padmanabhan, M. Jayachandra and H. J. Pandya, "Futuristic medical implants using bioresorbable materials and devices," *Elsevier,* vol. 142 Biosensors and Bioelectronics, 2019.

[4] M. P. Staiger, A. M. Pietak, J. Huadmai and G. Dias, "Magnesium and its alloys as orthopedic biomaterials: A review," *Elsevier,* vol. Biomaterials 27, pp. 1728-1734, 2006.

[5] T. Kokubo and H. Takadama, "How useful is SBF in predicting in vivo bone bioactivity?," *Biomaterials,* vol. 27, pp. 2907-2915, 2006.

[6] A. Rezaei and M. R. Mohammadi, "In vitro study of hydroxyapatite/polycaprolactone (HA/PCL) nanocomposite synthesized by an in situ sol-gel process," *Materials Science and Engineering C,* vol. 33, pp. 390-396, 2013.

[7] S. V. Dorozhkin, "Surface modification of magnesium and its biodegradable alloys by calcium orthophosphate coatings to improve corrosion resistance and biocompatibility," in *Surface Modification of Magnesium and its Alloys for Biomedical Applications*, Woodhead Publishing, 2015, pp. 151-191.

[8] R. M. Heiberger and E. Neuwirth, "One-Way ANOVA," in *R Through Excel*, Springer, 2009, pp. 165-191.

[9] L. Bland, A. King, N. Birbilis and J. Scully, "Assessing the Corrosion of Commercially Pure Magnesium and Commercial AZ31B by Electrochemical Impedance, Mass-Loss, Hydrogen Collection, and Inductively Coupled Plasma Optical Emission Spectrometry Solution Analysis," *Corrosion,* vol. 71(2), pp. 128-145, 2015.